

Integrated ultra-high-performance graphene optical modulator

ELHAM HEIDARI^{1,†}, HAMED DALIR^{2,†,*}, FARZAD MOKHTARI KOUSHYAR¹,
CHANDRAMAN PATIL², MARIO MISCUGLIO², DEJI AKINWANDE¹,
VOLKER J. SORGER^{2,*}

¹Microelectronics Research Center, Electrical and Computer Engineering Department, University of Texas at Austin, Austin, Texas 78758, USA

²Department of Electrical and Computer Engineering, George Washington University, Washington, DC 20052

*Corresponding authors: hdalir@gwu.edu sorger@email.gwu.edu

†These authors equally contributed to this work.

With the growing demand for massive amounts of data processing, transmission, and storage, it is becoming more challenging to optimize the trade-off between high-speed and energy consumption in current optoelectronic devices. Heterogeneous material integration into Silicon- and Nitride photonics has demonstrated high speed potential, but with millimeter-to-centimeter large footprints. The search for an electro-optic modulator that combines high-speed with energy efficiency and compactness to enable high component density on-chip is yet ongoing. Here we demonstrate a 60 GHz-fast (3-dB roll-off) micrometer-compact and 4 fJ/bit-efficient Graphene-based modulator integrated on Silicon photonics platform. Two dual Graphene layers are capacitively biased into modulating the waveguide mode's optical effective index via Pauli-blocking mechanism. The electro-optic response which is further enhanced by a vertical distributed-Bragg-reflector cavity, thus reducing the drive voltage by about 40 times while preserving an adequate modulation depth (~5.2 dB/V). Compact, efficient, and fast modulators enable high photonic chip density and performance with key applications in signal processing, sensor platforms, and analog- and neuromorphic photonic processors.

Introduction

Demand for increased data-handling performance in signal interconnects, optical transceiver

technology, and emerging applications such as photonic-based application specific integrated circuit (ASICs) for analog signal processing or neuromorphic computing and machine-learning acceleration [1] is driving a roadmap for continuous next-generation opto-electronic components [2] including component miniaturization for improved photonics integrated circuits (PIC) density [3]. The bandwidth-compression technique in electrical interconnects, for example, is failing to satisfy the increased demand in data processing and telecommunications mainly due to capacitive charging issues and thermal budgets. Both issues may be reduced by photonic interconnects by decoupling bit generation from data broadcasting and offers also multiplexing parallelization paradigms [4]. Electro-optic modulators are key components in the photonics circuits, which encode analog electrical into the optical domain by altering the effective refractive index (phase, frequency, polarization, or amplitude) propagation [5,6]. Their performance is determined by the device' response time (3dB roll-off speed), its drive voltage (power consumption), and physical footprint which contribute to PIC component density and utilization range in applications.

Silicon based modulators offer a mid-range performance with being 10's GHz fast (usually ≤ 50 GHz), but relatively bulky (O(~mm)) and higher voltage, due to its weak Pockels and Franz-Keldysh effect, but are monolithic to Silicon photonics [7,8]. Germanium-based modulators often have a high insertion loss and pose

monolithic complementary metal-oxide-semiconductor (CMOS) integration [9,10]. Lithium niobate's low material and waveguide loss offers for low drive voltages trading in footprint ($O(\sim\text{cm})$) [11]. As such, the search for an electro-optic modulator that demonstrates all key metrics is still ongoing.

Utilizing Graphene as the modulator material enables to address all device metrics; the high mobility allows for $\approx 50 \text{ Ohm}$ resistance. When combined with strong (beyond unity) optical index modulation at near IR frequencies, device footprints of less than 10 micrometer allow for sufficient signal modulation (e.g. extinction ratio) and rapid modulation due to low RC-delay. State-of-the-art speeds are around 30-40 GHz [12-14], however still fall short of the critical 50 GHz mark that is routinely offered by photonic foundries [AIM, AMF, IMEC]. Regarding system integration, Graphene development has shown CMOS compatibility with the demonstrated wafer-scale integration on silicon [15] and delivered high material thermal stability enabled by high thermal conductivity. This offers Graphene-based photonics to operated not only in cloud-systems, but also in network-edge gadgets [5,16]. When taken together, these properties and capabilities make graphene a prospective material for light-matter-interaction enhanced high-performance electro-optic devices for PIC integration.

Here we introduce a Graphene-based electro-absorption modulator integrated into silicon photonic waveguides capable of switching at 60 GHz, being micrometer compact (6 mm^2), and

highly efficient (4 fJ/bit). The low sub-voltage operation is achieved by (i) packaging a dual-graphene stack into a distributed Bragg reflector (DBR) which increases the light-matter interaction path-length, (ii) a low resistance of 50Ω to Graphene, and (iii) Graphene's natural strong index modulation from Pauli-blocking at near IR frequencies (here $\lambda = 1550\text{nm}$). The contributions of this demonstration rest in being the fastest graphene-based modulator in PICs to date, and demonstrating the novel paradigm of utilizing path length extension without compromising the footprint, which improve the energy efficiency by 40 times over the standard design [13].

Structure and Results

Fig. 1 (a) depicts the graphene optical modulator's schematic, which is based on a Bragg reflector waveguide design that is laterally merged with an α -Si waveguide. This modulator's planar integration is beneficial for ultra-dense on-chip optical interconnect applications. The DBR structure used in this design, is made up of a stack of alternating high and low refractive index layers, where the boundary conditions for each layer interface cause partial reflection of electromagnetic waves, and the grating period in DBR is designed to cause constructive interference between the reflected beams [17]. Owing to the top emission of the vertical-cavity surface-emitting laser (VCSEL) structure blocked by a thin film dielectric mirror, light propagates in a zigzag pattern to the modulator cavity [18,19].

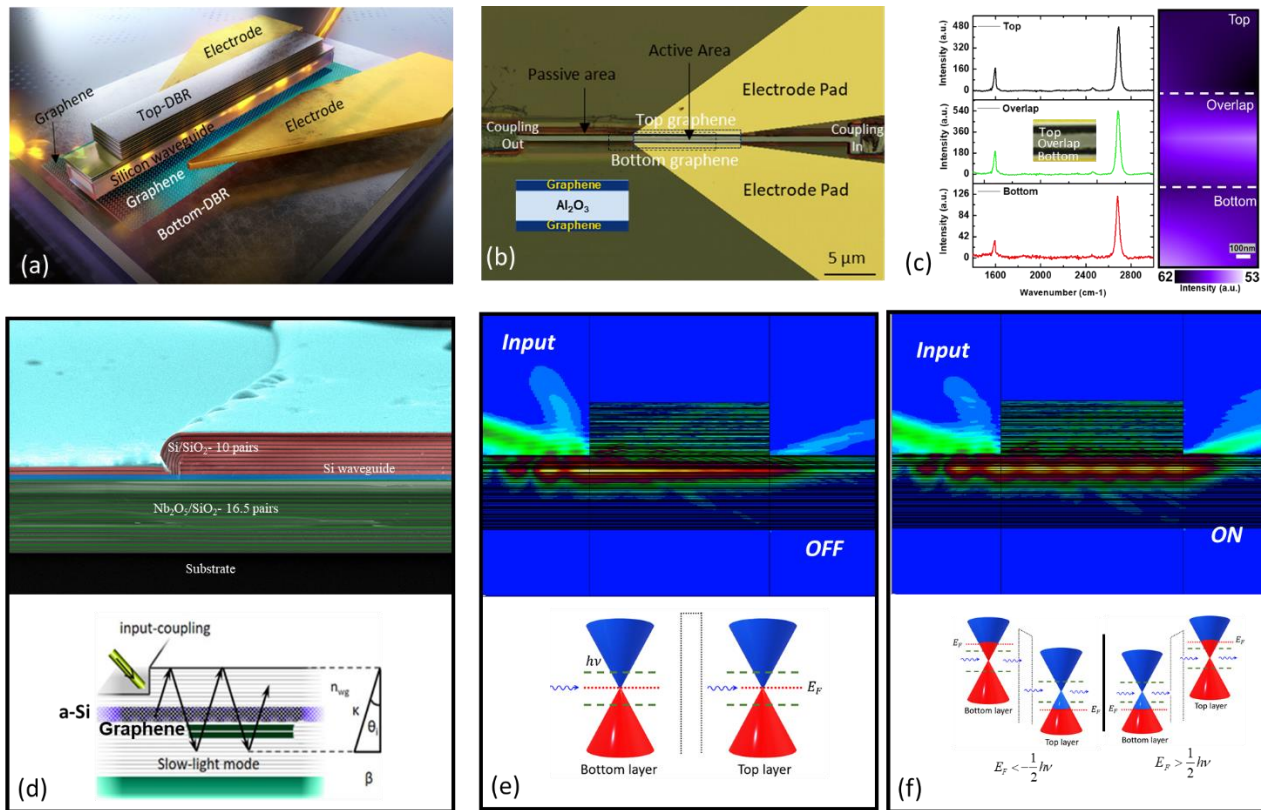


Fig. 1. (a) Three-dimensional schematic illustration of the ultra-high performance graphene optical modulator showing two layers of graphene are separated by interlayer of high- κ dielectric (Al_2O_3) to form parallel-plate capacitor. Top and bottom DBRs lead to a constructive interference between the reflected beams, (b) Top view microscopic image of the graphene optical modulator showing top view of the waveguiding, input/output couplers and electrode pads, (c) Raman mapping performed across channel showing intensity enhanced at the overlap region (microscope image as inset). (d(i)) Cross-section false-color SEM image of the fabricated graphene optical modulator, (d(ii)) Electric field distributions while excitation using a tilt-coupling scheme (e) Light-emission direction in the modulating cavity. The top emission of the modulator is prohibited by plating a thin-film dielectric reflectors, thereby light propagates to the modulator cavity in a zig-zag shape. EO modulator with un-doped graphene sheets leading Fermi level would be at the Dirac point under the illumination of photons with energy of $\hbar\nu$. In this case, the transmission would be heavily attenuated, and we called it as OFF state. Graphene's Fermi level distribution under OFF state is shown while the double layer graphene sheets are un-doped. Blue and red colors represent unoccupied and occupied states of Fermi level, respectively. (f) Electric field distribution in EO modulator with graphene's heavily hole or electron doped, which the state is called ON state; whereby inter-band transition is heavily suppressed, and transmission is allowed.

The top view optical microscopic image and cross section false-color scanning electron microscope (SEM) image of the graphene optical modulator are shown in Fig. 1(b) and 1(d(i)), respectively. On an InP substrate, 33 stacked pairs of $\text{Nb}_2\text{O}_5/\text{SiO}_2$ bottom DBRs are constructed. The graphene grown on the copper substrate is transferred to the fabricated bottom DBR to form the core with a planar graphene capacitor using the wet transfer method. Electron beam (e-beam) lithography is used to pattern the electrical contact to each graphene layer. The recommended Pd/Au (10/90 nm) electrode is deposited using an e-beam evaporator. The bottom graphene layer is patterned by e-beam lithography. After that, the undesired graphene is etched by plasma ashing, leaving only the patterned graphene. With e-beam evaporation, a thin coating of Al is deposited on the patterned graphene. A thin (20 nm) Al_2O_3 layer is placed on the structure using atomic layer deposition (ALD) for ultra-fast opto-electric applications and to prevent optical mode leakage. The width and thickness of the Si waveguide was designed to be $0.6\ \mu\text{m}$ and $0.445\ \mu\text{m}$, respectively, to ensure that a single transverse electric (TE) mode is propagated in waveguide. Plasma enhanced chemical vapor deposition (PECVD) was used to deposit an α -Si layer on the graphene and Al_2O_3 spacer, which was then e-beam lithographed. Two grating couplers are fabricated, which couples light into and out of the optical waveguide. Finally, 20 layers of Si/SiO_2 were deposited with a layer width of $\lambda/4n$, where λ and n represents wavelength and refractive index, respectively.

In other words, the Fabry-Perot interferometer is formed by the top and bottom DBRs. A core with a planar graphene capacitor consists of two graphene layers and a high-dielectric material, here Al_2O_3 , interlayer constructed beneath the silicon waveguide to assure the device's high-speed mechanism. The core's effective refractive index is higher than the top and bottom DBR mirrors' effective refractive indices. When a light wave strikes any interface, the angle of incidence exceeds the critical angle for total internal reflection (TIR) at either the bottom or top interfaces, causing the light to be confined and move in a zigzag pattern. The slow group velocity of light induced by light zigzag radiation considerably reduces the size of the optical device, boosting the device's performance, which is shown in Fig. 1(d(ii)).

Variations in the gate-controlled optical absorption in graphene induce changes in the optical modulator's transmission, which is controlled by changing chemical potential (μ , also Fermi level E_F) via an external gate field [20]. Electrical gating is used to control the absorption of graphene layers by electrodes connected to each graphene layer, as shown in Fig. 1(e,f) insets at bottom. Graphene's band structure is composed of two bands (valence band (π) and conduction band (π^*)) that degenerate at the so-called Dirac point.

The position of the Fermi level can be easily adjusted by changing the accumulation charge because of the low density of states. The Fermi level is at the Dirac point of all graphene layers in an undoped graphene, resulting in low insertion loss (see Fig. 1(e)). Charge transmission would be greatly affected if photons with less than $\hbar\nu$ energy were used to illuminate. This state is referred to "OFF" state.

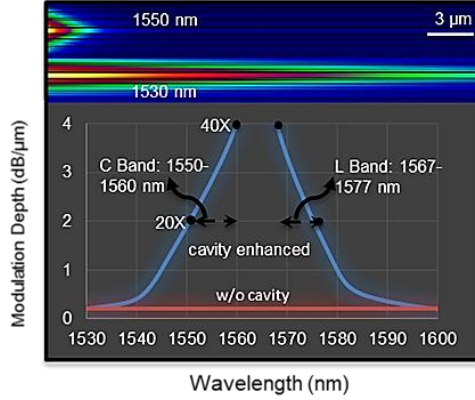


Fig. 2. Estimated modulation depth as a function of input-wavelength using film mode matching method of FIMMWAVE Photon Design Corporation. Top image shows the light guide in cavity in 1530nm and 1550 nm wavelengths.

While Fig. 1(f) represents an integrated double layer graphene hollow core waveguide in the “ON” state, when the graphene sheets are electron-, or hole-doped with emission of photons with the energy of $\hbar\nu$, and thus the Fermi level increases or decreases, respectively. Transmission between graphene bands is also possible when the Fermi level is changed by tuning the photon's half energy below or above the graphene's Dirac point. However, altering the bias voltage causes the Fermi level to shift below or over the threshold value ($\hbar\omega/2$), switching the optical inter-band transition ON or OFF.

The input wavelength can be used to modify the incident angle of the "zig-zag" light into the Bragg reflector waveguide, as shown in Eq. (1). Furthermore, the resonance wavelength is determined by the thickness of the α -Si waveguide squeezed between the mirrors (cut off condition: 1565 nm). As θ_i approaches 90 near the resonance condition, the interaction of light with graphene sheets rises dramatically, enlarging the absorption in the graphene layers.

$$\sin\theta_i = \sqrt{1 - \left(\frac{\kappa_z}{\kappa}\right)^2} = \sqrt{1 - \left(\frac{\lambda}{\lambda_c}\right)^2} \quad (1)$$

The modulator's performance is critical to the system's overall performance. High modulation speed, large modulation depth, small footprint, and low power consumption are ideal figures of merit (FOM) in the optical modulators. The modulation depth per micrometer of the device was estimated using FIMMWAVE Photon Design Corp.'s film mode matching approach in Fig. 2. At C- and L-band operation, a modulation depth of >4 dB per micron (> 40 dB for a 10 μm long modulator) may be achieved; although insertion loss increases marginally, which is proportional to the increased radiation loss of the DBR mirrors. According to the simulation results, for the on-chip integrated device, the insertion loss is estimated to be 0.7 dB.

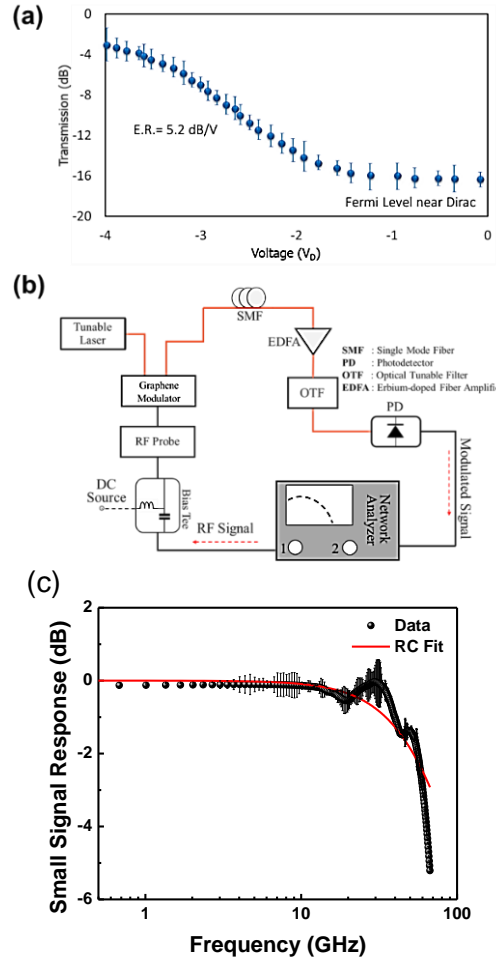


Fig. 3. (a) Electro-optical response of the device at different drive voltage. The modulation depth of the modulator is estimated to be 5.2 dB/V (b) In-house small-signal RF setup (S_{21} : ratio between optical amplitude modulation and RF signal), and (c) Normalized RF response of the double layer graphene optical modulator. The 3 dB cut-off frequency of 60 GHz was obtained.

Fig. 3(a) shows the photon transmission through the waveguide when different driving voltages (VD) are applied at a wavelength of 1.55 μm . The band structure of graphene is made up of two bands that degenerate at Dirac points. One of the properties of Dirac electrons in graphene is that the conductivity of the graphene-based structure changes dramatically when the electrons are confined. The position of the Fermi level in graphene can be easily modified by changing the accumulating charge due to the nature of the monolayer (low density of states).

The Fermi level is at the Dirac point in single-layer graphene that is undoped. The transmission would be reduced when photons with an energy of $\hbar\nu$ (where \hbar and ν denote the reduced Plank's constant and light frequency, respectively) were illuminated. Regardless, graphene's Fermi level decreases or increases in either hole- or electron-doped graphene sheets.

Fig. 3(b) shows the measurement setup schematic for the graphene optical modulator's small signal frequency measurement (S_{21}), which is obtained by generating a low power modulating signal (0 dBm) with an Agilent E8361 67 GHz vector network analyzer (VNA) and combining DC voltage bias with the RF signal with a 60 GHz bias tee. The voltage is applied between the top and bottom graphene layers. The light emitted into the modulator by a distributed feedback laser

(DFB) at 1550nm. A photodetector (PD, 60 GHz) with a broadband post-amplifier collects modulated light, which is then compared to the original modulating source.

The double-layer graphene modulator's dynamic response is shown in Fig. 3(c). The device's useable frequency range extends the optical 3dB (electrical 6dB) bandwidth up to ~60 GHz. The graphene modulator exhibits a 60 GHz small signal radiofrequency (RF) bandwidth, with an RC value restricted by graphene sheet resistance, capacitor size, and contact resistance. The total resistance is expected to be ~50 Ω .

Structure	Ref. #	Speed GHz	Footprint μm^2	Modulation Depth dB	IL dB	Energy per Bit fJ	Complexity
EO Plasmon	21	70	40	10	6	110	Moderate
SiGe	22	54	12	3.2	4	20	Hard
LiNbO ₃	11	45	20,000	18	0.4	14	Hard
G-Si	Here	60	6	5-11	4	4-10	Moderate

Table 1. FOM and performance comparison between existed designed/fabricated electro absorption modulators and proposed graphene modulators.

Considering the resistance of the modulator ~ 100 Ω (where 50 Ω comes from the measurement setup system) and $C=27$ fF, we can fairly elaborate the modulation response and power consumption ($E_{\text{bit}}=0.25CV^2$) of our device. A voltage swing of 0.57 V is necessary to modulate the device at 3dB. This voltage state uses about 2.25 fJ/bit of electricity for the switching operation.

While charge accumulation is sufficient to elevate the Fermi level with half of the photon's energy above (or below) the Dirac point, the inter-band transition is greatly suppressed, allowing for higher transmission. The strength of the coupling between the evanescent waves and graphene layers is adjusted by modifying chemical potential (also E_F) via an external gate field, which causes changes in graphene absorption, resulting in the optical modulator's transmission. Changing the bias voltage causes the fermi level to shift below or above the threshold value, allowing optical interband transitions to be turned on or off. Table 1 compares performances and FOM of previous proposed modulators and the proposed graphene modulator in this work.

Conclusion

Here, we demonstrate that by increasing the interaction of light with the graphene layer, by more than 40 times over the standard design, improving light absorption in graphene while reducing the power consumption. The electrical gating used here, adjusts the absorption of graphene layers through electrodes attached to each graphene layer. Because of the direct relationship between applied voltage and absorption in graphene, this device shows capability of sub-volt operation with a sufficient modulation depth (>5 dB). To move the Fermi-level from Dirac to the target point in the Pauli Blocking mechanism, only 2.25 fJ/bit power consumption is required. Due to the graphene's exceptionally high electrical and thermal conductivity, it would also be possible to operate at a fast speed. With the new platform, the device's speed is improved to reach ~60 GHz and beyond.

References:

- 1- M. Miscuglio & V. J Sorger, *Appl. Phys. Rev.* **7**, 031404 (2020).
- 2- M. M. Waldrop, *Nature* **530**, 144 (2016).
- 3- K. Liu, S. Sun, A. Majumdar & V. J. Sorger, *Sci. Rep.* **6**, 37419 (2016).
- 4- D. T. H. Tan, K. Ikeda, S. Zamek, A. Mizrahi, M. P. Nezhad, A. V. Krishnamoorthy, K. Raj, J. E. Cunningham, X. Zheng, I. Shubin, Y. Luo & Y. Fainman, *Opt. Express* **19**, 2401 (2011).
- 5- Q. Bao & K. P. Loh , *ACS Nano.* **6**, 3677 (2012).
- 6- Q. Cheng, M. Bahadori, M. Glick, S. Rumley & K. Bergman, *Optica* **5**, 1354 (2018).
- 7- P. Avouris , Z. Chen & V. Perebeinos, *Nat. Nanotechnol.* **2**, 605 (2007).
- 8- G. T. Reed, G. Mashanovich, F. Y. Gardes, & D. J. Thomson, *Nat. Photonics*, **4**, 518 (2010).
- 9- J. E. Roth, O. Fidaner, R. K. Schaevitz, Y.-H. Kuo, T. I. Kamins, J. S. Harris & D. A. B. Miller, *Opt. Express* **15**, 5851 (2007).
- 10- A. Liu, L. Liao, D. Rubin, H. Nguyen, B. Ciftcioglu, Y. Chetrit, N. Izhaky, & M. Paniccia, *Opt. Express* **15**, 660 (2007).
- 11- C. Wang , M. Zhang, X. Chen, M. Bertrand, A. Shams-Ansari, S. Chandrasekhar, P. Winzer & M. Lončar, *Nature* **562**, 101 (2018).
- 12- C. T. Phare, Y-H D. Lee, J. Cardenas & M. Lipson, *Nat. Photonics* **9**, 511 (2015).
- 13- H. Dalir, Y. Xia, Y. Wang & X. Zhang, *ACS Photonics* **3**, 1564 (2016).
- 14- D. Akinwande, C. Huyghebaert, C-H Wang, M. I. Serna, S. Goossens, L-J Li, H.-S. P. Wang & F. H. L. Koppens, *Nature* **573**, 507 (2019).
- 15- K. Kim, J. Y. Choi, T. Kim, S.-H. Cho & H.-J. Chung, *Nature* **479**, 338 (2011).
- 16- K. S. Novoselov, V. I. Fal'ko, L. Colombo, P. R. Gellert, M. G. Schwab & K. Kim, *Nature* **490**, 192 (2012).
- 17- P. Yeh, Wiley, ISBN: 978-0-471-73192-4, New York (2005).
- 18- H. Dalir, F. Koyama, *Appl. Phys. Express* **7**, 022102 (2014).
- 19- E. Heidari, H. Dalir, M. Ahmed, V. J. Sorger, & R. T. Chen, *Nanophotonics* **9**, 4743 (2020).
- 20- F. Wang, Y. Zhang, C. Tian, C. Girit, A. Zettl , M. Crommie & Y. R. Shen, *Science* **320**, 206 (2008).
- 21- M. Ayata, Y. Fedoryshyn, W. Heni, B. Baeuerle, A. Josten, C. Haffner, D. L. Elder, L. R. Dalton & J. Leuthold, *Science* **358**, 630 (2017).
- 22- J. Fujikata, M. Noguchi, et.al. *Opt. Express*, **28**, 33123 (2020).